

Determination of in-depth damaged profile by Raman line scan in a pre-cut He^{2+} irradiated UO_2

Cite as: Appl. Phys. Lett. **100**, 251914 (2012); <https://doi.org/10.1063/1.4729588>

Submitted: 06 April 2012 . Accepted: 29 May 2012 . Published Online: 22 June 2012

G. Guimbretière, L. Desgranges, A. Canizarès, G. Carlot, R. Caraballo, C. Jégou, F. Duval, N. Raimboux, M. R. Ammar, and P. Simon



View Online



Export Citation

ARTICLES YOU MAY BE INTERESTED IN

[In situ Raman monitoring of \$\text{He}^{2+}\$ irradiation induced damage in a \$\text{UO}_2\$ ceramic](#)

Applied Physics Letters **103**, 041904 (2013); <https://doi.org/10.1063/1.4816285>

[Raman spectra of oxides with the fluorite structure](#)

The Journal of Chemical Physics **59**, 1561 (1973); <https://doi.org/10.1063/1.1680227>

[Optical properties and electronic structure of \$\text{UO}_2\$](#)

Journal of Applied Physics **49**, 1463 (1978); <https://doi.org/10.1063/1.324978>

Applied Physics Reviews
Now accepting original research

2017 Journal
Impact Factor:
12.894

AIP
Publishing

Determination of in-depth damaged profile by Raman line scan in a pre-cut He^{2+} irradiated UO_2

G. Guimbretière,^{1,a)} L. Desgranges,^{2,b)} A. Canizarès,¹ G. Carlot,² R. Caraballo,³ C. Jégou,³ F. Duval,¹ N. Raimboux,¹ M. R. Ammar,¹ and P. Simon¹

¹CNRS/UPR3079 CEMHTI, 45071 Orléans Cedex 2 et Université d'Orléans, 45067 Orléans Cedex 2, France

²CEA/DEN/DEC Bat 352 Cadarache, 13108 Saint Paul lez Durance, France

³CEA/DTCD/SECM/LMPA, Marcoule 30207 Bagnols Sur Ceze, France

(Received 6 April 2012; accepted 29 May 2012; published online 22 June 2012)

Raman measurements were carried out to probe the spectroscopic signatures of the ion beam irradiation-induced damage and their in-depth profiles on a Uranium dioxide sample previously cut and polished prior to performing a 25 MeV He^{2+} cyclotron beam irradiation. Raman spectra clearly show the creation of three defects bands ($U_1 \approx 530$, $U_2 \approx 575$, and $U_3 \approx 635 \text{ cm}^{-1}$) resulting from the ion irradiation and also some changes in the T_{2g} peak of UO_2 . Their in-depth distribution inside the sample exhibits a clear increase of the damage from the surface up to the position of the implanted He. © 2012 American Institute of Physics. [<http://dx.doi.org/10.1063/1.4729588>]

Nowadays, elaboration processes or operating conditions require materials that can reliably withstand extreme conditions of radiation, and the compound being one of the most resistant to irradiation and the most important in terms of its applied physics context and their societal challenges is uranium dioxide (UO_2). Currently, UO_2 is the standard fuel used in light water reactors; therefore, increasing our fundamental understanding of this material over the broadest range of extreme conditions is essential for enhancing material performance and also for design and synthesis of new materials to address a broad range of future energy applications. During the core reactor irradiation or spent fuel storage, alpha decay of produced actinides induces “defects” at different scales (electronic, atomic, and mesoscopic). Understanding the links between the creation and the evolution of these defects, possibly precursors one to each other, remains a major scientific key-point in the knowledge of radiation damage in UO_2 . Unfortunately, the experimental study of the evolution of UO_2 under irradiation is complicated by the limited use of *in situ* characterization. Recently, an *in situ* Raman setup coupled with a cyclotron accelerator was developed at CEMHTI lab (Orléans, France).^{1,2} This unique experimental setup allows direct monitoring of the irradiation-induced changes of the samples in real time. Raman spectroscopy is known to be sensitive to the nature of chemical bonds in solids, and allows precise *ex situ* experiment by performing mapping with spatial resolution close to $1 \mu\text{m}$. Raman mapping was already performed for the structural characterization of irradiated/implanted materials such as 6H-SiC (Ref. 3) and $\text{Gd}_2(\text{Zr}_x\text{Ti}_{1-x})_2\text{O}_7$ pyrochlores.^{4,5} In these examples, the materials achieved a more or less amorphization state by irradiation. Many recent experimental works were devoted to Raman studies of uranium oxide compounds,^{1,2,6-12} however, very few are particularly dealing with Raman characterization of irradiated UO_2 .¹³ Thus, the first step in the Raman study is the precise identification

of the spectroscopic signatures characteristic of the structural damage resulting from ion beam irradiation of UO_2 . This identification is the scope of this letter.

A disc of sintered UO_2 ceramic (8 mm in diameter) was annealed at 1700°C in Ar/H_2 atmosphere in order to insure stoichiometry, and cut into two half-disks along the x-z plane with a small angle from the vertical. The obtained surfaces were then polished to obtain a mirror-like surface. In order to obtain analyzed surface with the same thermal profile than the bulk of the sample, the disk was reconstituted for limiting radiative losses from the analyzed surface during irradiation

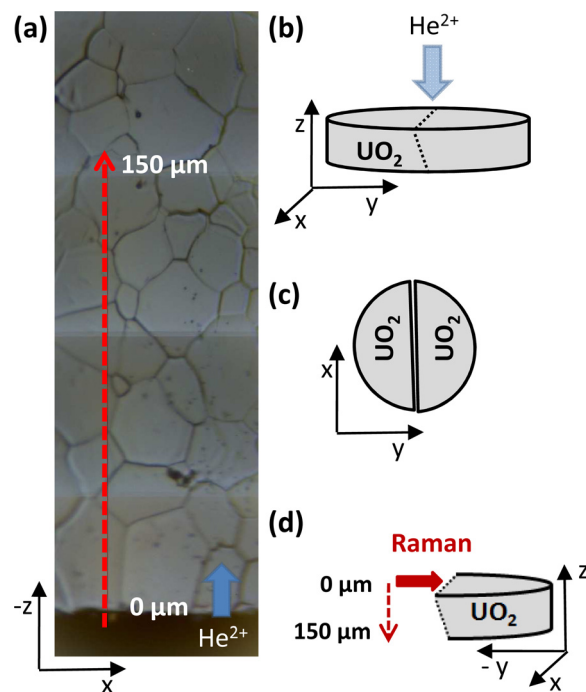


FIG. 1. Geometry of irradiation and Raman line scan of the irradiated pre-cut UO_2 sample. (b), (c), and (d) show the geometry of irradiation (in z direction) and Raman measurement (incident laser in y direction and line scan in the z direction, see (a) and (d)). The angle between the cut plane and the disk surface is close to 90° and is increased on Fig. 1(b) for sake of clarity.

^{a)}Electronic mail: guillaume.guimbretiere@cnrs-orleans.fr.

^{b)}Electronic mail: lionel.desgranges@cea.fr.

(Figures 1(b) and 1(c)). The sample was next irradiated under 10^{-6} mbar vacuum in order to avoid oxidation, with He^{2+} ions of ≈ 25 MeV produced by the CEMHTI cyclotron accelerator, in the DIAMANT device (alpha irradiation device for nuclear materials under temperature). Irradiation was performed with a flow of 200 nA for 2 h, which corresponds to a final fluence of 1.6×10^{16} He/cm^2 . *Post mortem* micro-Raman line scan measurements were performed at room temperature on the cross-section of the irradiated sample parallel to the He^{2+} ionic beam direction (z-axis, Figures 1(a) and 1(d)). Micro-Raman spectra were collected using a Renishaw Invia Reflex high-confocal spectrometer equipped with 633 nm of He-Ne excitation laser and a 1200 grooves/mm holographic grating allowing acquisition from 320 to 970 cm^{-1} . A $100\times$ objective was used with numerical aperture of 0.85, which gives spatial resolution better than $1 \mu\text{m}$. 776 spectra were required to map the analyzed area starting from $-5 \mu\text{m}$ up to $150 \mu\text{m}$ with a step of $0.2 \mu\text{m}$. The $0 \mu\text{m}$ value represents the border of the cut sample, i.e., the entrance side of the He^{2+} ions (see Figure 1). The small angle between the cut and xz planes allows probing the irradiation effect vs. depth: the analyzed sample is the one on the right side of Fig. 1(b), the induced damages are probed at the sample output.

Figure 2 pictures the whole spectra of the Raman scan in a color map representation. Their most prominent feature is the T_{2g} Raman-active mode appearing at 445 cm^{-1} characteristic of the fluorite structure of Uranium dioxide (see Figure 3).¹⁴ Additional bands also appear in the $500\text{--}700 \text{ cm}^{-1}$ range that progressively grow up from the surface ($0 \mu\text{m}$) up to $\approx 130 \mu\text{m}$.

Figure 3 shows the typical Raman spectra of virgin UO_2 acquired at the boundary (orange line) and inside (black line) a ceramic grain (see Figure 1), U_4O_9 phase (top red line), and implanted sample at the depth of $122 \mu\text{m}$ (black scatters). First, one can see that UO_2 “inside grain” spectrum exhibits only the T_{2g} band of undamaged structure (no pol-

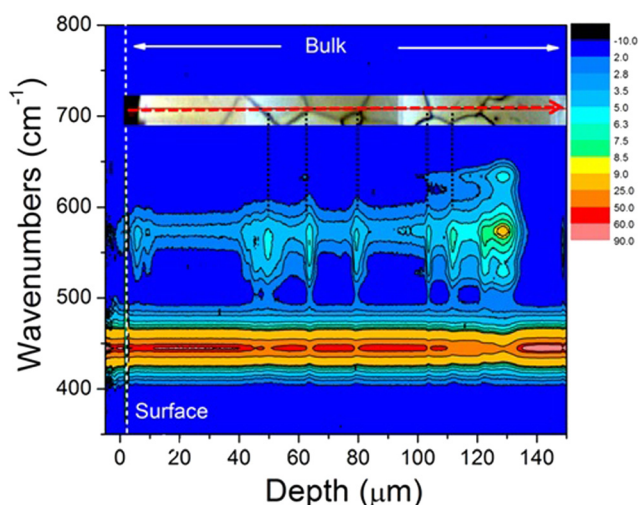


FIG. 2. Raman line scan of the irradiated pre-cut UO_2 sample: x axis is the depth scale, y axis is the wavenumbers, and Raman intensity in color. A zoom of the probed area in the picture of Figure 1 is added: dashed lines show the correspondence between grain boundaries and sharp peaks in Raman intensity.

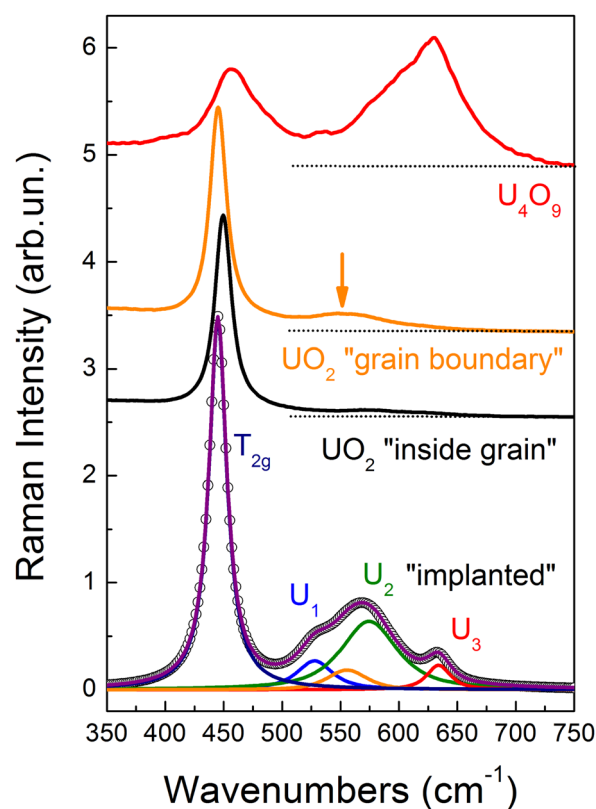


FIG. 3. Example of a typical Raman spectrum extracted from the line mapping ($122 \mu\text{m}$ position, in black). One can see the main T_{2g} peak of UO_2 (445 cm^{-1}) and the triplet of “defect peaks” due to irradiation ($U_1 \approx 527$, $U_2 \approx 574$, and $U_3 \approx 634 \text{ cm}^{-1}$). Spectra are deconvoluted with 5 Lorentzian peaks. The typical spectra of non-irradiated UO_2 at the center and boundary of grain ceramic and of U_4O_9 phase are also presented.

ishing effect), in agreement with theory and literature, whereas the spectrum of UO_2 “grain boundary” exhibits both the expected T_{2g} band and an additional broad band centered at 555 cm^{-1} (indicated by an arrow). Figure 3 shows also Raman spectrum of the “Implanted” UO_2 . This latter was deconvoluted in a classical procedure with a set of 5 Lorentzian bands: the T_{2g} band close to 445 cm^{-1} , the 555 cm^{-1} band, and a triplet of defect bands called U_1 , U_2 , and U_3 , in the range $500\text{--}700 \text{ cm}^{-1}$. It is worthy to note that the spectrum collected at $122 \mu\text{m}$ depth corresponds to a “grain boundary” position where the contribution of the 555 cm^{-1} band is not insignificant whereas this band completely disappears inside the grains. Such 550 cm^{-1} band has been already observed by Livneh in the case of UO_2 powder with no precise assignment¹² and we show here that is clearly not due to the only effect of irradiation.

Figure 4 presents the in-depth evolution of the output parameters (position (b), area (c), width (d)) of the T_{2g} peak and the areas of U_1 , U_2 , U_3 “defect peaks” (e). Additionally, the SRIM calculation of the depth of He implantation (black arrow) and theoretical distribution of energy deposit (dE/dx) by He^{2+} ions during irradiation (orange line) are added to the top of Figure 4(a).¹⁵ Compared to the values for unimplanted area ($<150 \mu\text{m}$ depth, dotted lines), the T_{2g} parameters and “defect peaks” areas exhibit the same shapes in depth with a plateau from the surface to about $100 \mu\text{m}$ and presence of an extremum whose depth matches the

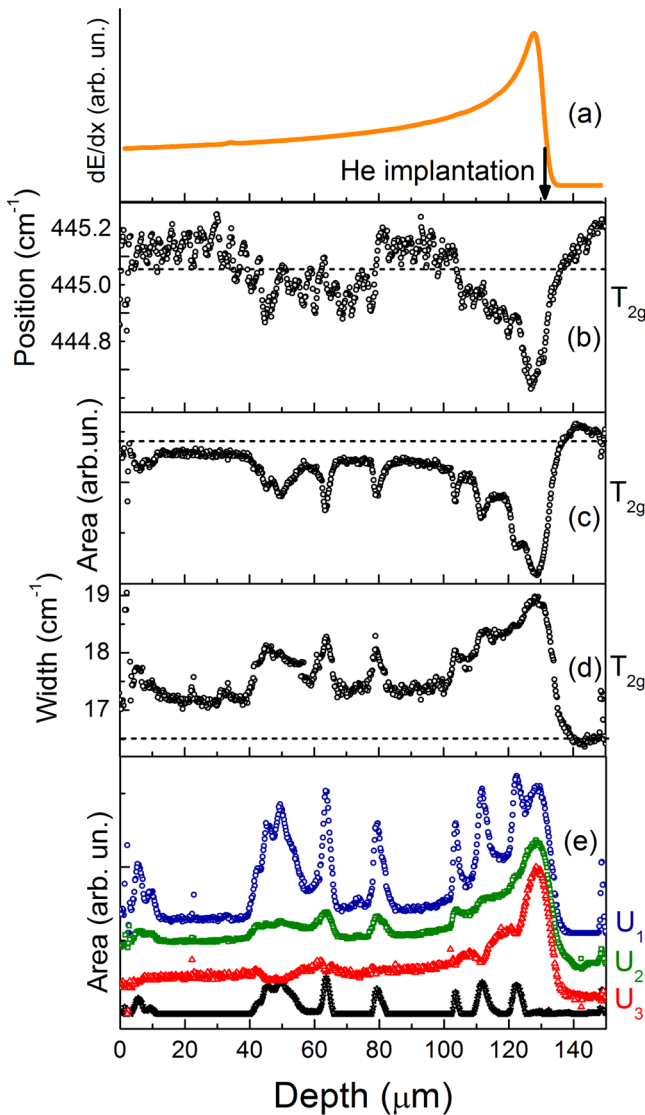


FIG. 4. Depth distribution of the T_{2g} parameter (position (b), area (c), and width (d)) obtained from deconvolution (see Figure 3). The top orange line in (a) is the SRIM calculated energy deposit depth profile dE/dx . (e) Depth distribution of the U_1 , U_2 , and U_3 area obtained from deconvolution. The black circles are the area of the 555 cm^{-1} band.

maximum of SRIM dE/dx profile. Although this shift is small (0.5 cm^{-1}), the spectrometer stability allows to evidence it. Then, He implantation clearly induces both the decrease of the T_{2g} bands position and area, as well as the increase of the T_{2g} linewidth. In the other hand, the positions and widths of the “defect peaks” appear to be quite constant in depth, with values $U_1 \approx 527.6 \pm 0.2$, $U_2 \approx 574.5 \pm 0.3$, and $U_3 \approx 634 \pm 0.1\text{ cm}^{-1}$ for positions, and $\Delta U_1 \approx 36.5 \pm 0.5$, $\Delta U_2 \approx 58.5 \pm 0.5$, and $\Delta U_3 \approx 24.2 \pm 0.2\text{ cm}^{-1}$ for widths. Presence of sharp peaks along the depth distribution of all parameters may be due to the fitting process: The “grain boundary” 555 cm^{-1} band is very close to U_1 and U_2 , and this proximity seems induce an overestimation of U_1 and U_2 band areas. Effectively, one can see on Figure 4(e) that the depth distribution of the 555 cm^{-1} band (pictured by black circles) matches perfectly the sharp peaks.

The procedure of pre-cutting and polishing of the ceramic sample before irradiation is *in fine* very efficient and

has allowed performing an accurate Raman scan of the irradiated UO_2 sample. This high resolution mapping reveals the spatial evolution of the defect bands from the surface entrance of He^{2+} ions up to the implantation area, where He atoms are trapped in the sample.

The defect bands are signatures of the structural modifications in UO_2 . An assignment of these defect bands can be postulated: the U_2 and U_3 peaks were already discussed in the frame of studies focusing on stoichiometry changes in UO_{2+x} samples^{7,9,11} and $(\text{U,Pu})\text{O}_{2-x}$ pellet,¹⁶ while a 540 cm^{-1} peak was observed in SIMFUEL specimens and assigned to a dopant oxide phase.⁶ Obviously, this latter assignment cannot explain the origin of the U_1 band in the case of pure irradiated UO_2 samples. In the present case, several indicators show that the appearance of these peaks is not ought to the surface oxidation (let us remind here that the irradiation was performed under vacuum): (1) Both U_2 and U_3 increase simultaneously while for stoichiometric effect the 574 cm^{-1} and 634 cm^{-1} bands intensity evolve in opposite trends.⁷ (2) It was also observed that the T_{2g} mode shifts to higher frequency with oxidation.^{7,10} Here, T_{2g} mode shifts to lower frequency with growth up of the “defect peaks.” (3) Shapes of distributions in depth of dE/dx and spectral signatures of irradiated UO_2 are similar, while no noticeable variations are observed in the unimplanted “bulk” area (from 140 to 150 μm). However, if the apparition of U_2 and U_3 peaks is not due to the surface oxidation, we argue that the structural changes at the origin of their appearance are similar: U_2 peak at about 575 cm^{-1} can be assigned to LO mode.¹⁷ This LO mode is Raman-forbidden in the unirradiated UO_2 (perfect fluorite structure) and becomes Raman-active due to a breakdown in the selection rules caused by the lattice damage and resulting from the implantation process.^{12,13} U_3 peak at about 635 cm^{-1} can be assigned to a structural defect of cuboctahedral symmetry as present in the crystalline structure of unirradiated U_4O_9 .⁸ The extinction of U_3 in HV crossed polarization measurement (not shown here) is consistent with this assignment. The assignment of the U_1 is less obvious, we postulate that local UO_{2+x} surstoichiometry defects observed through the U_3 band should be accompanied by local UO_{2-x} sub-stoichiometry defects. Then, U_1 band could be the Raman signature of such UO_{2-x} defects. The Raman activity of the Uranium oxides is known to be dependent of the energy of laser excitation,^{8,9,12} and this property can be at the origin of the non systematic observation of the three “defect peaks” in Uranium oxide compounds exposed to irradiation.^{13,16}

In summary, we have shown that pre-cutting of a ceramic oxide before irradiation can be an efficient way for Raman study of the irradiation effect without any mechanical effect due to *post mortem* cut and polishing performed after irradiation. Raman line scan on the edge of the irradiated UO_2 shows the absence of amorphization, and the large number of spectra (776) allows bringing out little spectral changes and precisely reconstructing the in-depth damage profile: intensity decrease, broadening and shift to the lower wavenumbers of T_{2g} peak, and the creation of three “defect peaks” signatures ($U_1 \approx 530$, $U_2 \approx 575$, and $U_3 \approx 635\text{ cm}^{-1}$). U_2 and U_3 peak are assigned to the same local structural modification than induced by deviation

from the exact UO_2 stoichiometry: U_2 is due to the activation of the Raman-forbidden LO mode. U_3 is due to a stoichiometric structural defect of cuboctahedral symmetry. U_1 may be the signature of sub-stoichiometric structural defect. All the peak parameters were plotted vs. depth and exhibit similar profiles, with a maximum of change at the depth of He ions implantation. Indeed, U_1 , U_2 , and U_3 modes have been observed previously in unirradiated chemically modified UO_2 compounds, but here, we highlight that under irradiation they simultaneously grow with He^{2+} slow-down. We can postulate that energy transfer and implanted He are at the origin of the observed Raman signatures: In one hand, implanted He is situated in associated defect sites or aggregated in bubbles. He gas is not Raman active, but it can be expected that during irradiation strain increases with implanted He concentration and should induce some modification of the T_{2g} band. The presence of this strain and He may then inhibit part of migration and annihilation of defects, leading to the formation of structural defects, like cuboctahedral ones, through processes of defects clustering and precipitation.¹⁸ In other hand, in the non implanted area, an increase of the lattice parameters¹⁹ induced by energy deposit should be at the origin of the presence of strain giving rise to the observed Raman signatures. Additionally, the presence of a 555 cm^{-1} band at the boundary of the grain ceramic is reported. This band of unknown origin is present in virgin UO_2 and is clearly stable with irradiation.

We expect that such experimental procedure (i.e., high resolution Raman probing of “defect peaks” behavior with depth on a pre-cut and irradiated ceramic) should be an efficient tool in the study of irradiation induced damage in materials.

The authors gratefully acknowledge GNR Matinex and EMIR network for financial support, as well Catherine Tanguy for her help in the synthesis of sample.

- ¹G. Guimbretière, A. Canizarès, M.-R. Ammar, P. Simon, M.-F. Barthe, Y. A. Tobon, and C. Corbel, *Spectrosc. Lett.* **44**, 570–573 (2011).
- ²A. Canizarès, G. Guimbretière, Y. A. Tobon, N. Raimboux, R. Omnée, M. Perdicakis, B. Muzeau, E. Leoni, M. S. Alam, E. Mendes, D. Simon, G. Matzen, C. Corbel, M. F. Barthe, and P. Simon, “*In situ* Raman monitoring of materials under irradiation: study of uranium dioxide alteration by water radiolysis,” *J. Raman Spectrosc.* (2012).
- ³F. Linez, A. Canizarès, A. Gentils, G. Guimbretière, P. Simon, and M. F. Barthe, “Determination of the disorder profile in an ion-implanted silicon carbide single crystal by Raman spectroscopy,” *J. Raman Spectrosc.* (2012).
- ⁴G. Sattonnay, S. Moll, L. Thomé, C. Decorse, C. Legros, P. Simon, J. Jagielski, I. Jozwik, and I. Monnet, *J. Appl. Phys.* **108**, 103512 (2010).
- ⁵S. Moll, G. Sattonnay, L. Thome, J. Jagielski, C. Decorse, P. Simon, I. Monnet, and W. J. Weber, *Phys. Rev. B* **84**, 064115 (2011).
- ⁶H. He, P. G. Keech, M. E. Broczkowski, J. J. Noël, and D. W. Shoesmith, *Rev. Can. Chim.* **85**, 702–713 (2007).
- ⁷H. He and W. D. Shoesmith, *Phys. Chem. Chem. Phys.* **12**, 8108–8117, (2010).
- ⁸L. Desgranges, G. Baldinozzi, P. Simon, G. Guimbretière, and A. Canizarès, *J. Raman Spectrosc.* **43**, 455–458 (2012).
- ⁹E. A. Stefaniak, A. Alsecc, I. E. Sajo, A. Worobiec, Z. Mathe, S. Torok, and R. Van Grieken, *J. Nucl. Mater.* **381**, 278–283 (2008).
- ¹⁰D. Manara and B. Renker, *J. Nucl. Mater.* **321**, 233–237 (2003).
- ¹¹S. D. Senanayake, R. Rousseau, D. Colegrave, and H. Idriss, *J. Nucl. Mater.* **342**, 179–187 (2005).
- ¹²T. Livneh and E. Sterer, *Phys. Rev. B* **73**, 085118 (2003).
- ¹³P. R. Graves, *Appl. Spectrosc.* **44**, 1665–1667 (1990).
- ¹⁴V. G. Keramidias and W. B. White, *J. Chem. Phys.* **59**, 1561–1562 (1973).
- ¹⁵J. F. Ziegler, J. P. Biersack, and U. Littmark, *The Stopping Power and Range of Ions in Solids* (Pergamon, New York, 1985).
- ¹⁶C. Jégou, R. Caraballo, S. Peugot, D. Roudil, L. Desgranges, and M. Maguin, *J. Nucl. Mater.* **405**, 235–243 (2010).
- ¹⁷J. D. Axe and G. D. Pettit, *Phys. Rev.* **151**, 676 (1966).
- ¹⁸A. Debelle, A. Boulle, F. Garrido, and L. Thomé, *J. Mater. Sci.* **46**, 4683–4689 (2011).
- ¹⁹N. Ishikawa, T. Sonoda, Y. Okamoto, T. Sawabe, K. Takegahara, S. Kosugi, and A. Iwase, *J. Nucl. Mater.* **419**, 392–396 (2011).